Journal of Building Engineering 117 (2026) 114713

Contents lists available at ScienceDirect

Journal of Building Engineering

journal homepage: www.elsevier.com/locate/jobe

Full length article

# Experimental investigation of acoustic airtightness measurement and UAV-based quantitative infrared thermography for building energy performance assessment

Philip Groesdonk *, Benedikt Kölsch, Björn Schricke, Markus Diel, Nirav Patel, Bernhard Hoffschmidt

*German Aerospace Center (DLR), Institute of Solar Research, Jülich/Cologne, Germany*

ARTICLE INFO

*Keywords:*
Airtightness
Thermography
UAV
Building envelope characterization
Measurement

ABSTRACT

In existing buildings, knowledge about the thermal envelope, its physical parameters, and possible hidden defects is often insufficient. This issue contributes to the performance gap between modeled and actual energy efficiency of existing buildings. Furthermore, reliable data about the existing structure is essential for cost-efficient retrofit strategies to reduce operational costs and carbon emissions. As a consequence, improving on-site measurements could offer new strategies to address the performance issues and promote efficiency measures. In an experimental investigation, this study explores two innovative methods applied to an exemplary building complex: acoustic air leakage detection and quantitative UAV-based infrared thermography. For acoustic leakage detection, the method effectively discerns the airtightness quality of large buildings but lacks sufficient automation and accuracy for robust quantitative evaluation. The drone-based thermography method featuring repeated coverage of a building over the course of a night holds promise for large-scale thermal assessment, but faces high equipment requirements, difficulties in precise image positioning, and challenges in integrating thermal data into 3D building models. Moreover, environmental factors such as wind, temperature gradients, and drone-induced turbulence introduce uncertainties that complicate reliable quantification. These challenges underscore the need for improved calibration procedures, advanced processing algorithms, and integration with dynamic building performance simulation. Despite these obstacles, the methods demonstrate promise for large-scale applications, with potential to automate and enhance energy performance assessments in future research.

## 1. Introduction

The building sector plays a pivotal role in global energy consumption and, consequently, in the emission of greenhouse gases. The ambitious reduction targets for greenhouse gas emissions, set at various governmental levels, demand significant contributions from all sectors responsible for emissions [1], including the building sector. Given the current political goals, the pace of $CO_2$ emission reduction in this sector needs to catch up [2]. Implementing efficiency measures, such as building energy renovations and the transition to renewable energy sources, is essential for the sector's alignment with these environmental goals. These measures not only address the immediate challenges, but also positively impact planning security. With the expected rise in the prices of

* Corresponding author.
*E-mail address:* philip.groesdonk@dlr.de (P. Groesdonk).

https://doi.org/10.1016/j.jobe.2025.114713
Received 1 April 2025; Received in revised form 4 November 2025; Accepted 18 November 2025
Available online 24 November 2025

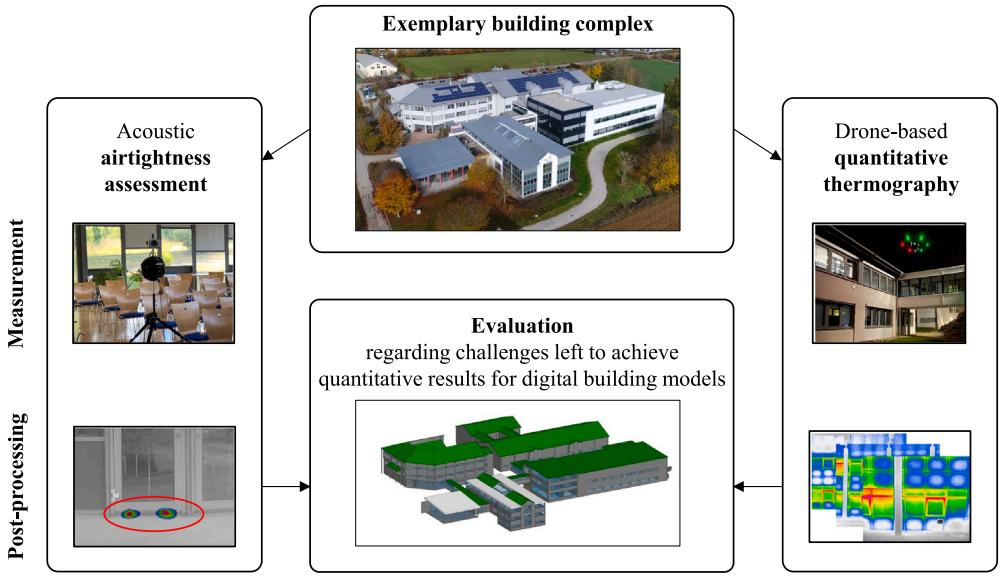


**Fig. 1.** Overview of the case study and methods applied within the study.

fossil fuels in the future and the increasing influence of energy efficiency on property values, these measures become even more pertinent [3].

Currently, the annual renovation rate of buildings in the European Union is just 1% [2] and needs to be increased for several reasons. While a detailed exploration of these reasons, as done e.g. by Konstantinou and Dimitrijević [4], is beyond the scope of this paper, it is essential to note that building owners have a vested interest in understanding the energy efficiency of their properties. This understanding allows them to identify weaknesses and to make informed decisions for future developments. Accurate predictions of savings from planned measures are essential. This necessitates (a) thorough analysis of the current state of the building to understand the reasons for its existing energy use and (b) precise prediction of the energy demand in the planned state. For effective fault detection and user influence modeling, accurate and affordable models of building physics are necessary. To minimize the cost barrier, the effort for creating such models should be as low as possible.

A significant portion of the uncertainty in the difference between modeled energy demand and actual usage comes from issues related to building physics. Mirroring the points listed above, they may result from (a) properties of the actual fabric of the building before retrofit not included in the model parameters and/or (b) differences between retrofit plans and implementation (as-planned vs. as-built).

This study explores and evaluates the applicability of innovative contact-less measurement technologies for building energy performance assessment. These technologies aim at detailed analyses in unrefurbished buildings and at post-renovation quality control, which significantly contribute to the performance gap between predicted and actual savings.

We applied two innovative, contact-less measurement methods to an exemplary building complex, as shown in Fig. 1. We demonstrate the use of acoustic airtightness assessment with an internal sound source and an external acoustic camera. Moreover, we discuss a drone-based thermography method, designed to measure spatially distributed surface temperatures multiple times in a single night. These methods are promising due to the possibility of characterizing the building envelope as a whole with regard to the two main reasons for heat losses: air exchange and thermal conduction. A research building complex with heterogeneous age and construction types as well as non-optimal performance in airtightness and insulation provided an ideal case for testing.

In the paper, we present the insights from this pilot application, focusing primarily on the challenges of modeling within the analysis of measurement results. We aim at finding the challenges left to reach quantitative results that can be automatically integrated into digital building models and therefore connected to building performance simulation.

The paper starts with a review of the literature and the state of the art. Afterwards, we introduce the case study building complex and explain the two measurement methods in detail. After presenting the findings of our pilot application, we draw conclusions regarding the challenges and recommendations for future improvement of the approaches.

### *1.1. Literature review and state of the art*

The goal of reducing the difference between modeled energy demand and energy use is probably as old as building performance simulation. Scholars have found various reasons for the so-called energy performance gap since then [5–8]. Factors identified to contribute to this gap include occupant behavior, device specifications, and wasted energy, but also uncertainty in building physics parameters and poor workmanship. In low-energy buildings, modeled energy demand tends to underestimate energy use [7], causing operational costs to be higher and retrofits to pay out later than expected.

Unintentional air exchange through a building's envelope is a significant concern, accounting for an estimated 30–50% of a building's heating and cooling energy use [9–12]. Such unintentional airflow is a major contributor to heat loss, underscoring the need for effective airtightness measures. For instance, Bracke et al. [13] demonstrated that improving air permeability from approximately $16\,m^3\,m^{-2}\,h^{-1}$ to $5\,m^3\,m^{-2}\,h^{-1}$ at 50 Pa can result in a 31–35% reduction in heat loss. Similarly, Leprince et al. [14] showed that reducing air permeability from $3\,m^3\,m^{-2}\,h^{-1}$ to $1.2\,m^3\,m^{-2}\,h^{-1}$ at 4 Pa can decrease energy consumption by 13–37%, depending on the ventilation system. This corresponds to annual energy savings of $6–17\,kW\,h\,m^{-2}$, highlighting the significant role of airtightness improvements in reducing both thermal losses and overall energy consumption.

Thermal transmittance governs the heat transfer through the building envelope, thus being an obvious contributor to energy performance. Rodrigues et al. [15] demonstrate this by varying U-values and building geometries in different climate conditions, resulting in an impact of up to 88% on energy demand.

A prerequisite for implementing contact-less measurements in an automated workflow is the existence of a spatially referenced 3D building representation. With the growing importance of building information modeling (BIM) in construction projects, also for retrofits, generating such models has been a topic of extensive research and development works. 3D laser scans, photogrammetry, and the more or less automated generation of BIM models from the resulting point clouds can be considered state of the art [16]. Using these models for energy applications in automated processes, e.g. exporting them to building performance simulation software, is a topic with several open challenges [17] beyond the scope of this paper.

This study focuses on the aspect of improving the model values regarding building physics parameters by contact-less measurements. As a consequence, this section aims to summarize the state of the art of such technologies, particularly regarding airtightness and thermal transmittance.

#### *1.1.1. Airtightness measurement*

The fan pressurization method, also known as the blower-door test and described in ISO 9972 [18], is commonly applied to measure airtightness. While this method is widely recognized, it comes with its set of challenges [19,20]. Identifying and quantifying leaks, especially during renovations, is crucial yet difficult using standard methods, including the blower door test. These methods are not only time-consuming, but also depend heavily on the expertise and experience of the energy consultant conducting the test.

In addition to methods like smoke sticks, tracer gas detection [21], or infrared scanning [22], the ASTM E1186-17 [23] standard, builds up on the work of Keast and Pei [24], suggests the use of sound detection for leak identification. However, its application in building scenarios remains limited.

Several studies explore sound transmission losses through building envelopes in laboratory [25–28] and field settings [29,30] to quantify leakage sizes with varying degrees of success. Exploring beyond the audible sound range, Graham [31] investigates infrasonic impedance measurements for leakage detection, while other researchers focus on localizing [32–34] and quantifying [35,36] air leakages in buildings. Recent advances include the use of microphone arrays and beamforming techniques for a comprehensive assessment of building façades and leak localization. Raman et al. [37] and Chelliah et al. [38,39] propose the near-field acoustic holography method for locating and quantifying leaks in buildings and building components. Janotte et al. [40] use the acoustic method in combination with other technologies, such as radar, infrared thermography, and $H_2$ tracer gas techniques, to explore more efficient and accurate assessments of existing buildings.

In our study, we apply the acoustic measurement method in addition to infrared thermography to assess buildings on a large scale. This dual approach aims at providing a more holistic and effective means of evaluating and improving building airtightness.

#### *1.1.2. Quantification of thermal transmittance*

For assessing building heat loss, several calculation-based, non-contact-less, and invasive methods exist. Furthermore, infrared thermography (IRT) has been widely used for qualitative or quantitative analysis of surface temperatures and the related thermal parameters. In the following, the state of the art in close-range IRT for buildings is presented after briefly describing other methods for heat loss quantification, summarizing the details given in a doctoral thesis related to this work [41].

In their *Review of in situ methods for assessing the thermal transmittance of walls*, Bienvenido-Huertas et al. [42] conclude:

> The theoretical estimation method [(ISO 6946 [43])] is often used in energy audits because no tests are required (the main advantage of this method) [and] because the composition of a wall can be assessed using various methods, such as [...] (i) endoscopy, (ii) using reliable technical documentation or databases describing the envelope of the building of interest, or (iii) using estimates based on analogous constructions.

As a consequence, this method has different disadvantages depending on its implementation. It is either (i) destructive, (ii) requires substantial a-priori knowledge that may have to be manually obtained from old plans, or (iii) is not necessarily representative for the observed building. Bienvenido-Huertas et al. [42] continue:

> In situ measurements can give more representative values [...], but the use of such methods is affected by many factors, with environmental factors being the most important. In situ measurement methods require [...] (i) a high thermal gradient ($T_{in} - T_{out} > 10\,°C$), (ii) a wind speed of 0–1 $\frac{m}{s}$, (iii) zero rainfall, and (iv) no solar radiation or other radiation sources to affect the wall of interest.

The mentioned in-situ methods for U-value measurement include the heat flow meter method standardized in ISO 9869-1 [44], a simple hot-box heat flow meter method that creates a small volume with controlled temperature on one side of the wall, and a thermometric method that measures the interior surface temperature in addition to environment temperatures on both sides. All of them require the installation of measurement equipment on the walls, access to the building interior, and a measurement period of more than a day.

Of particular interest for this paper are the **quantitative infrared thermography (QIRT)** methods. They may also be performed from the interior, but it is their implementation from the exterior that enables a high variability and automatability including image acquisition from UAVs, even though the environmental requirements regarding temperature differences and gradients, wind, and solar radiation are demanding. This is also found by Patel et al. [45] in an uncertainty analysis of a practical application of exterior QIRT. Therein, they build up on steady-state estimation methods such as the one presented by Dall'O' et al. [46] who use the equation

$$U = h_{\mathrm{comb,out}} \cdot \frac{T_{\mathrm{s}} - T_{\mathrm{air,out}}}{T_{\mathrm{air,in}} - T_{\mathrm{air,out}}} \tag{1}$$

to derive the $U$-value from the measured surface temperature $T_{\mathrm{s}}$, the air temperatures inside $T_{\mathrm{air,in}}$ and outside $T_{\mathrm{air,out}}$ and the combined (i.e. including radiation and convection) heat transfer coefficient $h_{\mathrm{comb,out}}$. As a matter of fact, $h_{\mathrm{comb,out}}$ is heavily influenced by the local conditions, including surface properties and wind. Similar procedures, with partly different equations, measured values, and assumptions for $h_{\mathrm{comb,out}}$ are presented by e.g. Madding [47] and Bayomi et al. [48]. Videras Rodríguez et al. [49] build up on Bayomi et al.'s calculation approach and calculate accurate U-value measurements from drone thermography of the same region repeated every quarter of an hour, combined with interior surface temperature measurements.

As a consequence of the dynamic nature of heat loss, Patel et al. [50] develop a dynamic method for quantifying wall parameters from multiple IRT recordings. They calibrate the parameters of a resistance–capacitance (RC) wall model to the surface temperature readings from a stationary infrared camera over a time range of five days. Influences from the surroundings are reduced by covering the investigated wall with a tent. Mahmoodzadeh et al. [51] manage to quantify and reduce important uncertainty contributions to infrared-sourced quantitative thermal performance assessment. In a follow-up work, they identify challenges and opportunities in quantitative aerial thermography of building envelopes as a response to various inconsistencies in published studies. Among others, they find camera temperatures affected by UAV-induced turbulence imply an important uncertainty contribution. They conclude that a robust protocol for quantitative thermal assessment of building envelopes requires additional research by both camera manufacturers and users [52].

Publications about QIRT on buildings mainly focus on how to reduce uncertainty of the measurement results. The reason for this is the challenging task of extracting the desired surface temperature from the sensor output. It requires the removal of additional influences to the value. Looking at the physical background of the involved phenomena, we can express the recorded value in a simplified way as

$$L_{\mathrm{sensor}} = \tau_{\mathrm{atm}} \cdot \left(L_{\mathrm{obj}}\left(T_{\mathrm{s}}\right) + L_{\mathrm{r}}\right) + L_{\mathrm{atm}} + L_{\mathrm{cam}} \tag{2}$$

with the contributions shown in Fig. 2: $L_{\mathrm{sensor}}$ is the radiance recorded by the sensor. $L_{\mathrm{r}}$ is the reflected ambient radiance. $\tau_{\mathrm{atm}}$ and $L_{\mathrm{atm}}$ are the transmittance and emitted radiance respectively of the atmosphere between object and sensor. $L_{\mathrm{cam}}$ is the radiance emitted by the camera housing onto the sensor.

$$L_{\mathrm{obj}}\left(T_{\mathrm{s}}\right) = \varepsilon_{\mathrm{obj}}\left(\vartheta_{\mathrm{o}}, \varphi_{\mathrm{o}}\right) \cdot L_{\mathrm{bb}}\left(T_{\mathrm{s}}\right) \tag{3}$$

is the radiance emitted by the object of interest at its surface temperature $T_{\mathrm{s}}$ and depends on the blackbody radiation at that temperature $L_{\mathrm{bb}}\left(T_{\mathrm{s}}\right)$ as well as on the directional emissivity of the object towards the sensor $\varepsilon_{\mathrm{obj}}\left(\vartheta_{\mathrm{o}}, \varphi_{\mathrm{o}}\right)$. Although infrared cameras usually display their recordings as temperature values, radiance is the quantity actually measured. In fact, the phenomena described above are spectral phenomena. The sensor integrates the incoming radiance weighted by its own spectral responsivity. Finally, the camera software derives a temperature value from the result [53–55].

While publications about QIRT mainly focus on how to reduce measurement result uncertainty, **qualitative thermography** has reached impressive results recently. For example, Rakha et al. [56] demonstrate the texturing of a 3D building model with infrared images recorded in five flights during a single night as a prerequisite to diagnose thermal anomalies in different size and shape. This shows the ability of state-of-the-art UAV equipment and photogrammetry methods to connect IR readings with 3D building models.

## 2. Materials and methods

In the following, we introduce the building complex we use as a pilot case for the methods. Furthermore, we explain both the acoustic air leakage detection method and the drone-based infrared thermography method in detail.

### 2.1. Selection of the building complex

The building complex shown in Fig. 3 provided a suitable test case for the methods under investigation due to several advantageous characteristics. Its structure includes building parts constructed between 1989 and 2019, offering a heterogeneous age profile that allows for testing on components with varying insulation qualities. The location further shows its suitability, with limited surrounding vegetation and no directly neighboring buildings ensuring access for drone operations.

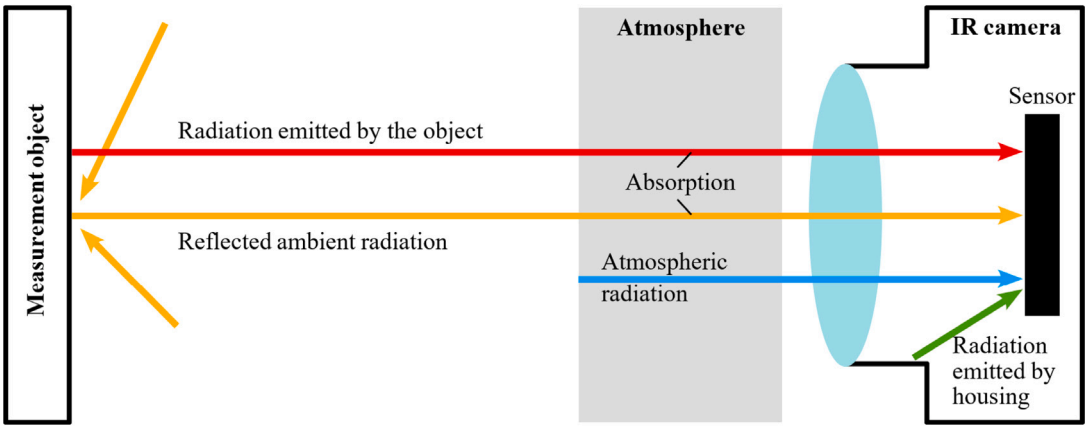


**Fig. 2.** Contributions to the radiation recorded by the IR camera sensor.

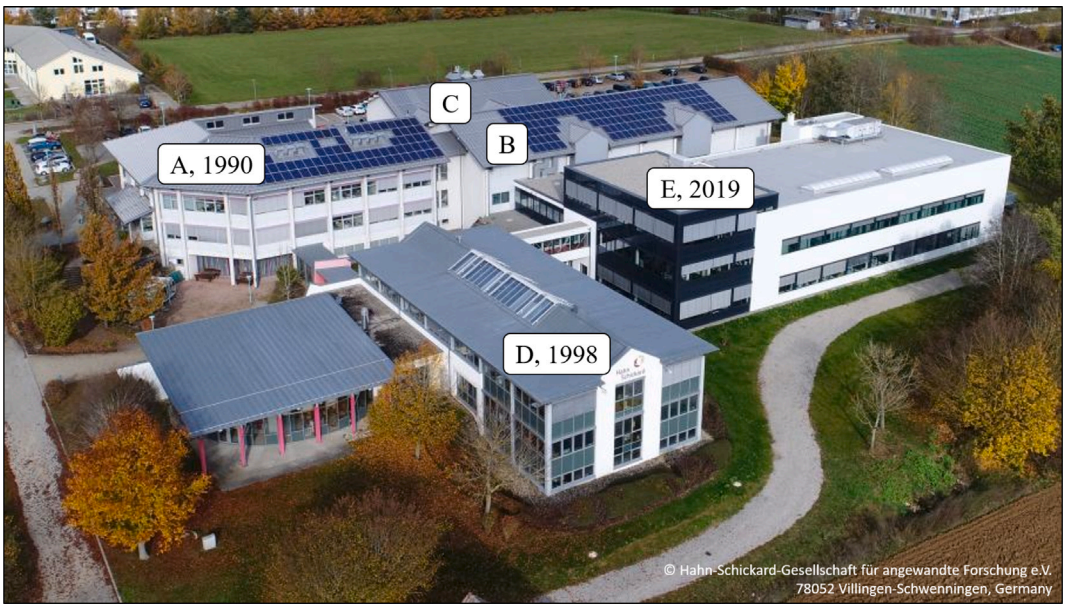


**Fig. 3.** The building complex with building names and years of construction or renovation.

### *2.2. Acoustic air leakage detection methodology*

The acoustic air leakage detection method is based on a microphone ring array, often referred to as an acoustic camera, consisting of 48 uniformly distributed microphones arranged in a circular array with a diameter of 0.75 m. The array operates in a frequency range of 164 Hz to 20 kHz. At its center, an optical camera with a resolution of 1920 × 1080 pixels captures visual images of the observed scene, complementing the acoustic measurements. The experimental setup and resulting images are shown in Fig. 4 (steps 2 and 3).

The methodology involves positioning the loudspeakers inside the building (Fig. 4, step 1), and the acoustic camera outside the building on the opposite side of the wall (Fig. 4, step 2).

Two loudspeakers were utilized: a high-frequency speaker operating in an even frequency range of 15–120 kHz and a low-frequency dodecahedron speaker covering a range of 0.05–16 kHz. Sound waves emitted by the loudspeakers penetrate through leaks in the wall and are detected by the acoustic camera on the exterior side, where the leaks are identified and localized as secondary sound sources.

For this study, a computer-generated white noise signal at a sound pressure level of 85 dB was emitted inside the building for a duration of four seconds. The resulting acoustic data was processed using the software NoiseImage (Fig. 4, step 3), employing the power beamforming technique to improve image clarity and enhance the precision of source representation. Additional details on the measurement procedure, experimental setup, and data evaluation can be found in Schiricke et al. [57].

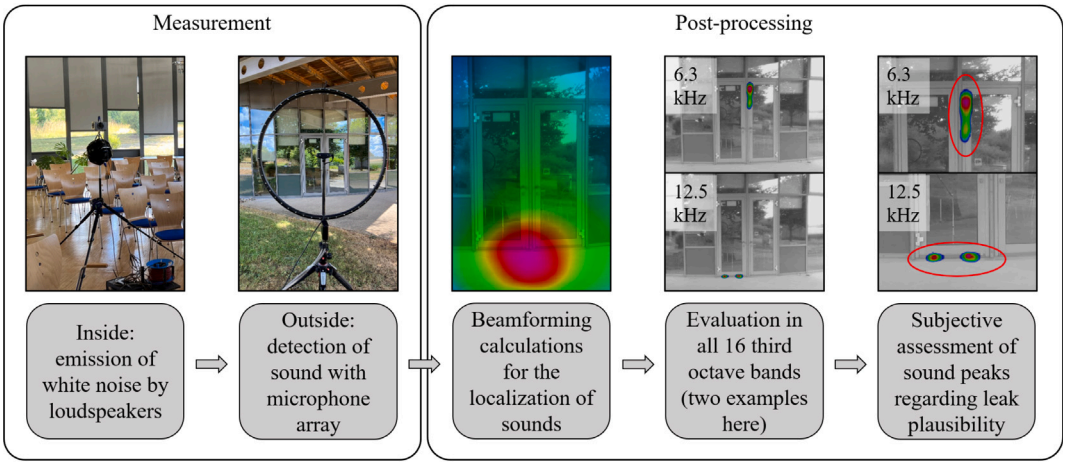


**Fig. 4.** Illustration of the experimental acoustic setup and the steps of the post-processing.

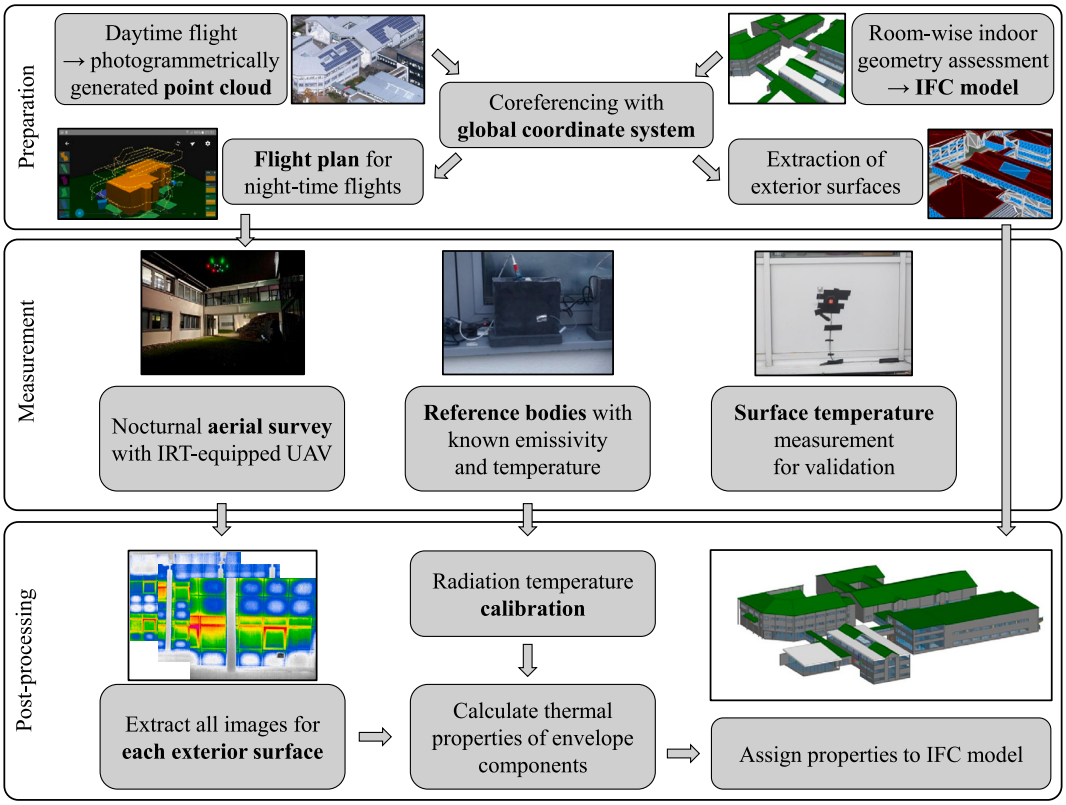


**Fig. 5.** Illustration of the experimental setup and the steps of the drone-based infrared thermography approach.

### *2.3. Drone-based infrared thermography method*

In addition to the airtightness evaluation, we investigate a drone-based infrared thermography approach for quantitative assessments of the building envelope. This includes an overview of the preparations and the used equipments, the flight procedure, and the data collection from the images. Fig. 5 visualizes the steps of the approach.

**Fig. 6.** The UAV system applied for the pilot application, with the thermal camera attached via gimbal.

*2.3.1. Preparation*

Before the thermal measurements, the preparation steps shown in Fig. 5 were conducted. An IFC model of the building, which in this case was generated independently of the flight campaign using a hand scanner [58], is coreferenced with a photogrammetric point cloud from a daytime flight. This ensures a common (globally referenced) coordinate system between the IFC model and the subsequent IRT flight. The externally visible surfaces are then extracted from the IFC model. This process is not trivial, and there is no standardized procedure for it [59]. Our experimental application uses a simplified geometric analysis based on the Python interface of IfcOpenShell and requires manual post-processing.

*2.3.2. Night-time IRT flight and image texture extraction*

The flight over the building complex was conducted at night. This approach offers several advantages. The most relevant for the accuracy of the measurement is the absence of sunlight. Furthermore, there is little or no need to consider building operations. Changes in conditions caused by users (e.g. opened windows, changes in room temperature) can be ignored.

The system used for the flight (pictured in Fig. 6) consists of the DJI M600 Pro drone, the Gremsy S1 gimbal, and the Workswell Wiris Pro uncooled microbolometer thermal camera (640 × 512 pixels, spectral range 7.5–13.5 µm, accuracy ±2 K).

The assignment of images to external surfaces (part of the post-processing in Fig. 5) requires the geometric co-evaluation of the IFC model surfaces and the thermal camera's position and orientation. The latter needs to be known with very high accuracy. Common GPS data cannot fulfill these requirements without corrections. One possibility is the use of RTK-GPS. It needs additional equipment and the geometry between the antennas and the camera (including 3-axis distance, gimbal rotation, drone tilt etc.) to be considered, which requires substantial effort if not provided by the manufacturer [60]. As a remedy, we opted for a software-based solution. Photogrammetry software is able to optimize the position in the process of creating a 3D point cloud from the data [61]. The software can take preliminary knowledge about the measured object from the flight plan and GPS positions into account. It optimizes image positions and orientations to create a fitting three-dimensional point cloud. The corrected image metadata are subsequently available as a byproduct [62].

*2.3.3. Quantitative image evaluation*

The purpose of evaluating the infrared images is to quantify the surface temperature of the measurement object. For this, other contributions to the radiation recorded by the sensor must be corrected for in the measured value. As shown in Eq. (2), this includes (i) the emissivity of the surface, (ii) the reflected ambient radiation, (iii) the influence of the atmosphere between surface and camera, and (iv) effects of the optics and the imaging sensor itself.

A complete consideration of all these phenomena at the measurement site is considered not feasible. Spectral differences within the wavelength range of the sensor are particularly difficult to handle. As mentioned in Section 1.1.2, the spectral sensitivity of the sensor is a suitable weight factor of integral values. For the phenomena listed above, we apply simplifications to Eqs. (2) and (3) known from literature:

(1) Surfaces have constant (but material-dependent) emissivity $\varepsilon_{\mathrm{obj}}$ when viewed not too obliquely [63]: $\varepsilon_{\mathrm{obj}}\left(\vartheta_{\mathrm{o}}, \varphi_{\mathrm{o}}\right) = \varepsilon_{\mathrm{obj}}$

(2) The measurement object is a Lambertian reflector, so the reflected ambient radiation $L_{\mathrm{r}}$ can be determined by attaching crumpled aluminum foil that is considered an ideal reflector [64]: $L_{\mathrm{r}} = L_{\mathrm{foil}} \cdot (1 - \varepsilon_{\mathrm{obj}})$

(3) We neglect the atmospheric influence, which mainly arises from water and carbon dioxide components in the air. In the sensitivity range of the sensor, it is very small at the short observation distances and low dew point temperatures with values of $\tau_{\mathrm{atm}} > 0.999$ (calculated using the Passman–Larmore tables in Gaussorgues [65]).

(4) Experience shows that realistic absolute values can be achieved only if calibration is carried out in the field. One countermeasure to obtain values of $L_{\mathrm{cam}}$ varying over time is to use reference bodies treated with a paint of known emission properties and whose surface temperature is continuously measured. Ideally, these bodies should represent the upper and lower limits of expected radiation values of the measurement objects [50].

Considering all these simplifications and Eqs. (2) and (3), we get

$$L_{\mathrm{bb}}\left(T_{\mathrm{s}}\right)=\frac{L_{\mathrm{sensor}}-L_{\mathrm{foil}}\cdot\left(1-\varepsilon_{\mathrm{obj}}\right)-L_{\mathrm{cam}}}{\varepsilon_{\mathrm{obj}}} \tag{4}$$

to derive blackbody radiance (and thereby surface temperature) from sensor readings.

#### 2.3.4. U-value calculation

With the steps explained above and shown in Fig. 5, a texture of the 3D building model featuring multiple surface temperatures measured over the course of the night can be created. From this, thermal transmittances of all building parts can be fitted using dynamic wall models (as done by Patel et al. [50]). The component under consideration is represented by a resistance-capacity model (RC model), which is widespread in building performance simulation. This contrasts with established methods that calculate U-values based solely on individual measurements, assuming constant conditions in the wall (see Section 1.1.2). An open question is how complex the dynamic model can be, given the small value of <10 measured temperature values over the course of the night. Furthermore, uncertainty heavily depends on the various influencing factors mentioned above. Glass parts are particularly complicated to measure due to their low emissivities and direct reflection of infrared radiation. For now, we focus on opaque building parts and uniform, non-metallic surfaces.

## 3. Findings and discussion of challenges and recommendations

The application of the methods described above to the case study building complex allowed us to evaluate their potential for the assessment of large-scale buildings. In the following, we present our findings and discuss the challenges and recommendations derived from it regarding both methods separately.

### 3.1. Acoustic air leakage detection

The present study involved a comprehensive analysis of 57 acoustic measurements taken across 36 rooms. Consequently, hundreds of potential leaks were located and visualized across the large area of the investigated building complex. The veracity of several leaks was confirmed through the utilization of conventional methods, including the employment of smoke sticks.

While the evaluation of these leaks enabled differentiation between buildings in terms of their airtightness quality, the high degree of manual evaluation involved poses a significant challenge that cannot be overlooked. In order to advance the development of measurement technology, the authors propose large-scale measurement campaigns to be conducted both in the field and in the laboratory. This would facilitate a more in-depth investigation into the management of sound reflections and noise suppression, and the identification of potential solutions.

#### 3.1.1. Findings

The detected sound sources indicating potential leakages primarily fell within a spectral range of 800 Hz to 25 kHz. To enhance visualization, only the highest sound pressure levels ($\Delta$ dB) within each of the 16 third-octave frequency bands were superimposed on visual images (Fig. 7).

As observed, sound peaks can manifest at various positions within different frequency bands, suggesting potential leaks at diverse locations (compare Fig. 4, step 4). Displaying all leakages simultaneously in one image is seldomly feasible. Typically, a sequence of images across different frequency bands is required to depict the detected potential leaks in the building envelope.

While sound peaks often indicated leaks, some arose from sound reflections or structure-borne vibrations, as demonstrated by the vibration of a window pane in Fig. 7, which is evidently situated in an implausible location for a leakage and is more likely attributable to the vibration of the pane.

However, in numerous instances, a visual examination at the positions of the sound peaks validated credible reasons for air leaks. Two examples are shown in Fig. 7, where (left) a drilled hole from a previously installed window and (right) a cable fairlead to the blind coincided with the position of the sound peak. These two examples of acoustically detected potential leakages were confirmed by the use of a blower door and a smoke stick.

Frequently though, the origin of a sound peak could not be definitively verified due to constraints in time resources. Consequently, these sound peaks necessitated a subjective assessment regarding their plausibility in relation to potential leakages (compare Fig. 4, step 5). For this purpose, the plausibility of a leakage as the cause of the sound source was assessed in each case on the basis of the exact position of the sound peak, following the method presented in the work of Schiricke et al. [57]. The assessment is based on a set of subjective criteria ranging across four levels from “very likely” to “very unlikely”. Consequently, the Acoustic Assessment Score (ASS) was introduced as a quantitative metric for every detected sound peak. Along with the ASS, a color code was assigned to each sound peak. The criteria can be summarized as follows: “Very likely leakage” (ASS=3, red): The peak of the signal is located at a particularly plausible site, such as the seals of door and window frames. “Likely leakage” (ASS=2, yellow): The peak of the signal is at a plausible location, such as joints between different materials, or even at a particularly plausible site, though it has a much weaker signal. “Unlikely leakage” (ASS=1, gray): There are some indications that the signal is probably not caused by a leakage, or the peak being near but just off a plausible location. “Very unlikely leakage” (ASS=0, white): The peak of a signal is at an implausible location, such as on a window pane.

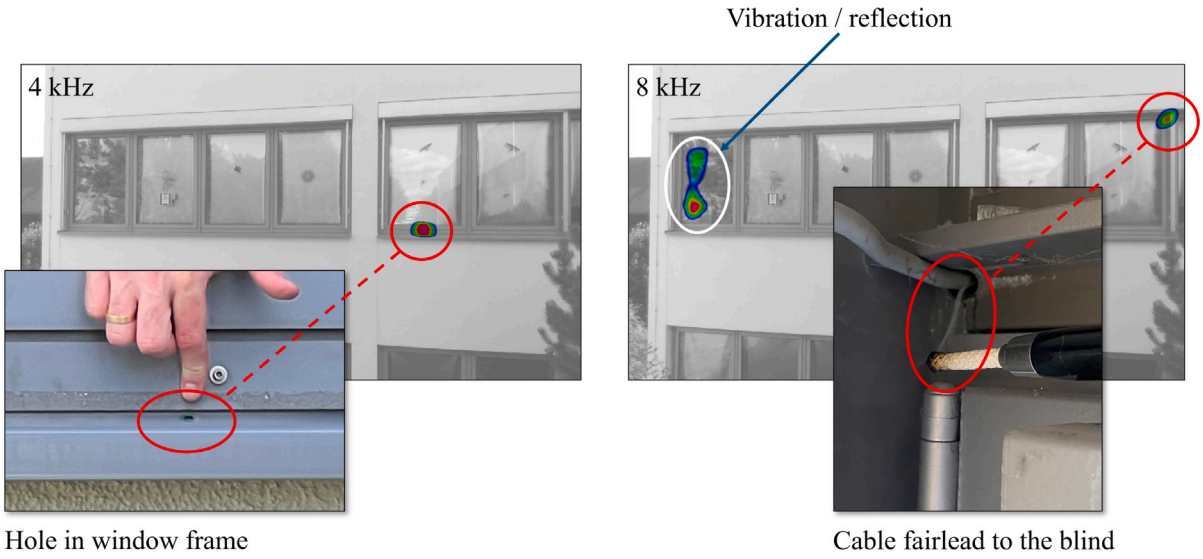


**Fig. 7.** Examples of detected leakages.

**Table 1**
Overall assessment of the acoustic leakage analyses for the three buildings.

| MFAS | No. of measurements per building | | |
|---|---|---|---|
| | D (1998) | A (1990) | E (2019) |
| Very low (0–9) | 0 | 3 | 3 |
| Low (10–19) | 8 | 10 | 4 |
| Mid (20–29) | 10 | 2 | 3 |
| High (30–39) | 13 | 0 | 0 |
| Very high (40–48) | 1 | 0 | 0 |

This approach facilitated the documentation of the assessments in the façade representation, utilizing the corresponding color code to pinpoint potential leakage locations on the façade (alike in Fig. 4, step 5 and Fig. 7) for inspection and subsequent sealing if needed. For a detailed example of how potential leaks are assessed and graphically represented using the above criteria and color codes, please refer to Figure 3 in Ref. [57].

On the other hand, the ASS was employed to evaluate and compare the airtightness of different rooms, leading to the creation of the Multi-frequency Assessment Score (MFAS). This quantitative metric for a specific room's airtightness was subsequently utilized to compare the three buildings.

Table 1 illustrates the frequency distribution of the obtained MFAS for the various measured rooms in the three buildings D, A and E (compare Fig. 3). This overview serves as a means to evaluate whether the applied acoustic method was successful in discerning differences among the buildings. As anticipated, building D, recognized as problematic by the building owner although not the oldest structure, exhibits the highest values in the MFAS, which indicates a strong acoustic evidence of leakage and, thus, a poor airtightness rating.

Similarly, as depicted in Fig. 7, the acoustic camera was able to detect leaks on a large window front. The recorded image is presented in Fig. 8. Two leaks are evident, with the one situated at the midpoint of the window on the left being corroborated by the presence of protruding window paneling with a seal. The signal peak in the top right of the window front could be attributed to a slight damage to the window seal. The sound pressure level was then determined using the evaluation software NoiseImage, across the specified frequency range, at the two identified peaks. The results are displayed in Fig. 9. A comparison of the two curves within the range in which the leaks can be clearly seen (approximately 4 kHz to 8 kHz) reveals a notable difference in monotony. The question of whether different causes of leakage exhibit disparate characteristics within the spectrum, thereby enabling the identification of the specific type and severity of the leakage based on these characteristics, is currently under investigation at the test stand described by Diel et al. [66].

These findings are encouraging with regard to the acoustic approach to the airtightness test. The question thus arises as to how one might proceed from this qualitative and partly subjective assessment to a quantitative (and potentially automated) evaluation in the subsequent step. To this end, a test facility has been developed, which allows for the systematic investigation of different types of leakage under laboratory conditions, as well as different operating parameters. The test facility itself as well as the results of first measurements are described in Diel et al. [66]. In order to make quantitative statements about airtightness using acoustic


**Fig. 8.** Detected leakages at a large window front. The frequency range from 5.4 kHz to 6.0 kHz was selected to superimpose the sound pressure level on the photograph.

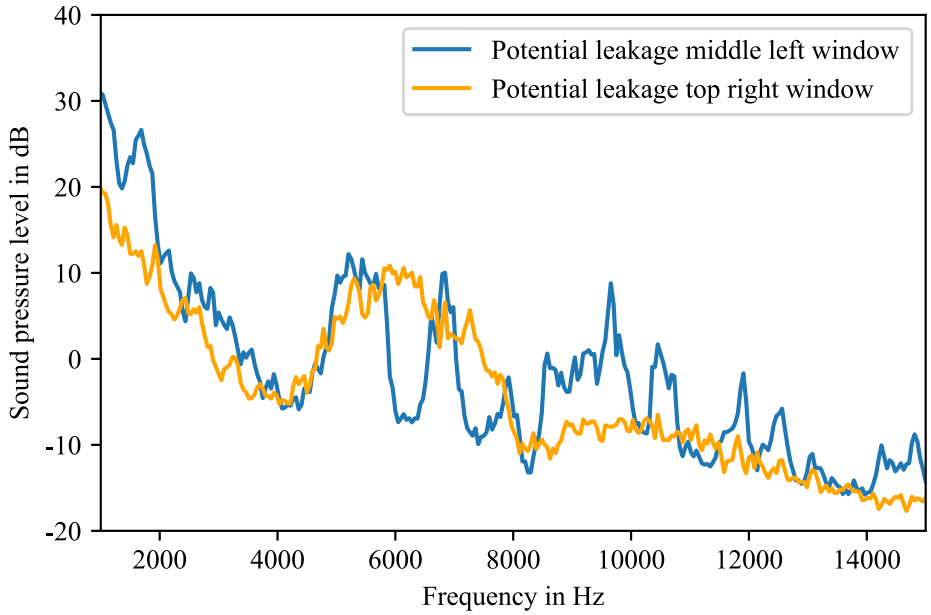


**Fig. 9.** Sound pressure level over time for the two detected potential leakages from Fig. 8.

measurements, the relationships between acoustic signatures and an associated measure of airtightness (such as the air volume flow at a pressure difference of 50 Pa) are to be examined in particular.

### *3.1.2. Discussion of challenges and recommendations*

This field study has offered valuable insights into the practicality, speed, and interpretability of acoustic signals, as well as the method's scalability and potential for future advancements. The results indicate that a substantial number of potential leaks can be identified, affirming the method's fundamental effectiveness for large buildings. Additionally, a comparison of the distribution of the ASS and the MFAS within the various buildings suggests that the applied acoustic method successfully differentiated the airtightness quality among the three buildings.

Challenges to be solved involve increased automation in identifying pertinent locations. Connecting the images to a 3D building model or applying image segmentation could support this by adding semantic information to the objects examined. This underscores

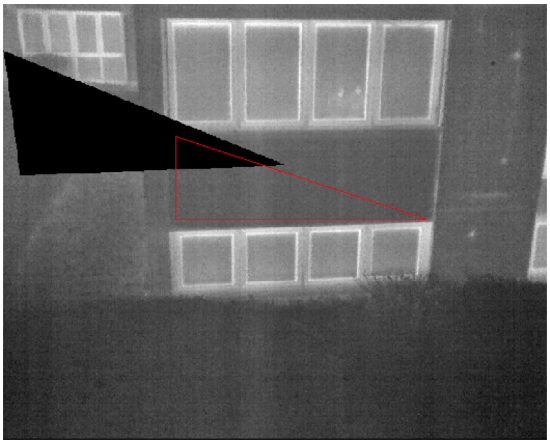

**Fig. 10.** Element texture extracted by analyzing camera position and IFC model coordinates (black), compared with element marked on the image (red).

the necessity for systematic laboratory or field investigations involving known instances of leakage. The potential of this methodology is considerable. Promising future developments include noise reduction through reference signals [34], utilizing acoustic spectra to deduce the type and size of leaks [35,36], and employing multi-perspective analysis to eliminate reflections. Moreover, visualizing leaks across different third-octave frequency bands in a unified image could enhance the effectiveness of the leak detection process. Looking ahead, we anticipate conducting more thorough examinations at testing facilities and renovation sites. There are also plans for improvements in measurement technology, including the integration of infrared thermography with the current acoustic camera setup to enhance the reliability of leak detection. Additionally, exploring the development of a suitable ultrasonic transmitter is another area of consideration.

### *3.2. Drone-based infrared thermography*

The method pictured in Fig. 5 and explained in Section 2.3 features multiple flights over the entire building complex. Through automated texturing, all images need to be assigned to the pictured building parts as surface textures in the 3D model. Subsequently, their radiation values are converted to surface temperatures. In the next step, these values serve to determine the RC parameters of the building parts.

Due to several issues in the experimental application, we were not able to demonstrate the full workflow. In the following, we explain the issues that we found hindered successful processing. Furthermore, we present results from the manual evaluation of the data to enable an analysis of challenges left to achieve reliable quantitative results.

#### *3.2.1. Automatic processing*

The most relevant issues in the process described in Section 2.3.2 arose during image acquisition. The pre-planned flight routes with the recommended overlap of 80–90% [61] could not be flown autonomously due to safety concerns. Unfavorable wind conditions and small distances between trees and the façade in some places posed a high risk for collisions. As a consequence, the drone was operated manually for flight control and image triggering, resulting in two major setbacks for the evaluation:

(1) Significantly less building area was covered by images than planned. Instead of monitoring the whole complex, we focused on parts A and D (see Fig. 3).
(2) Preliminary knowledge for each image position and orientation would have been a by-product of the pre-planned flight route. Without it, the photogrammetry software could not accurately correct the drone's GPS position data—neither based on the thermal data nor on the simultaneously recorded, poorly lit optical data.

The latter issue is visualized in Fig. 10. The red triangle marks the surface part of the IFC model that should have been textured from the image. The black triangle is the section of the image that would have been used when inferring the pictured object from the IFC coordinates and the metadata about position and orientation from the image file. With the apparent deviation, automated texturing of surface parts from the IRT imagery becomes impossible.

On the positive side, the drone provided a significantly longer battery life (>45 min) compared to the manufacturer's specifications (20 min) due to the low flight dynamics and despite ambient temperatures of about 0 °C.

The issues described above provide important insights into necessary improvements of the experiment setup. Nevertheless, they are not immanent to the method itself. Therefore we selected images for exemplary further processing and extracted regions of interest manually from them.

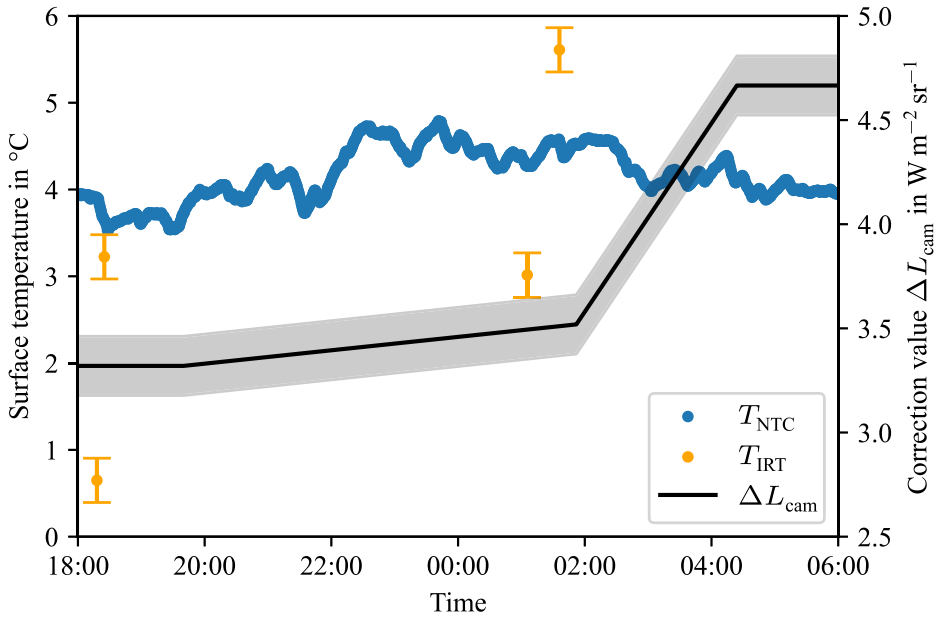


**Fig. 11.** Correction values for $L_{cam}$ from blackbody measurements and comparison between surface temperatures measured by thermography and by NTC contact thermometer on an example façade, with error indicators ($1\sigma$) restricted to short-time influences.

*3.2.2. Quantification through manual evaluation*

In this section, we present findings from the manual evaluation of the infrared recordings acquired during the drone flights. Illustrated by exemplary results from the on-site application, we evaluate the potential and the shortcomings of the demonstrated approach and present learnings for future research.

The reference bodies were positioned on the flat roof of the side wing of building D (see Fig. 3). They were imaged several times within a few minutes with the infrared camera at around 7:40 pm, 1:52 am and 4:24 am. From the comparison of measured surface temperatures and recorded radiation values, we derived correction factors for $L_{cam}$. They translated to temperature differences of 5–10 K, increasing over the course of the night (see Fig. 11). For images recorded within a few seconds, with the bodies shown in different pixels, we observed variations of ±0.25 K. While the former value is significantly higher than the manufacturer's value for the thermal camera accuracy, the second is significantly lower. This supports previous findings with stationary cameras that the availability of a reference value enables quantitative evaluations.

For application on images taken in between, the $L_{cam}$ correction values were interpolated and applied to derive surface temperatures as described in Eq. (4). Fig. 11 shows a comparison of the surface temperature determined with an NTC (negative temperature coefficient) contact and the presented thermography method at the north façade of the building complex, as shown in Fig. 5 in the middle. The error bars of the thermographic temperature values illustrate the influence of the ±0.25 K mentioned above (for scattering within a short timeframe, as a mean value over the three reference body observation periods) and do not include any further uncertainties in the measurement result. These ranges do not reach the actual surface temperatures by far and absolute values vary significantly over time, indicating that this issue is a major obstacle for reliable on-site calibration.

Our findings show that occasional calibration with the reference body is not suitable for the task, as it cannot cover the variations mentioned above. Another indicator for this is the point cloud in Fig. 12: Although the images used for the grayscale texture were taken within several minutes and internal camera correction was fixed to plausible values, the figure shows substantial temperature variations with no apparent physical reason on the building. A possible explanation is the effect that also Mahmoodzadeh et al. [52] find: Changes in the housing temperature caused by varying environmental conditions heavily influence the sensor. Given the inevitable variations in convective heat transfer due to airstream during the flight and in wind conditions due to weather and building structure, we conclude that each image's uncertainty needs to be treated directly, e.g. by further calibration of each thermographically obtained value.

Due to the small number of sampling points and the high measurement uncertainty, we did not calibrate an RC model to the measured surface temperatures. For the values given in Table 2 along with the measurement results according to standard ISO 9869-1 [44] with heat flow sensors, we use Eq. (1) with temperature differences averaged over the measurements and a standard value of $h_{comb,out} = 13.4\,W\,m^{-2}\,K^{-1}$, determined according to Dall'O' et al. [46]. As a further comparative value, we add an application of the same equation to surface temperatures measured by contact (NTC) thermometers and recorded every two hours. From Eq. (1) it is immediately clear that the choice of heat transfer coefficient and the measured outside air temperature have a major influence on the result, as also stated by Patel et al. [45] in their sensitivity analysis. It is not possible to give a realistic uncertainty for the tabulated values, which is why we did not include them in the table. The values given should only be taken as examples and by no means to evaluate the method presented.

**Fig. 12.** Point cloud textured with infrared imagery.

**Table 2**
Determined U-values from measurement and from model application to surface temperature measurement results. The values given are for demonstration purposes and are not intended to evaluate the method presented.

| Method | $U$-value in $\mathrm{W\,m^{-2}\,K^{-1}}$ |
|---|---|
| Measurement according to ISO 9869-1 [44] | $1.21 \pm 20\%$ |
| Model application to thermographic measurements | 1.1 |
| Model application to NTC temperature values | 1.4 |

### *3.2.3. Discussion of challenges and recommendations*

The advantages of the UAV-based quantitative infrared thermography system presented are numerous. It has the potential to record data on the insulation quality of medium-sized building complexes for which hand-held thermography is no longer realistic (e.g. office buildings, schools or administrative headquarters) in a short space of time and to link the results directly to the building geometry and model semantics.

Thermography challenges to tackle are inaccurate image positioning, automated IFC/BIM processing with regard to areas to be analyzed, and a significant improvement in the accuracy of thermography, in particular regarding on-site correction of varying environmental influences. Regarding the latter, weaknesses in the design of this study are to be revised. In particular, the calibration of the camera with the reference bodies proved to be insufficient. If the problem of the fluctuating accuracy of the camera cannot be solved at hardware level, reference values may be required in (almost) every image. Contact temperature sensors on every examined surface would significantly increase the effort required for data acquisition and thus partially negate the advantages of the system. Another possibility is a shielded camera as proposed by Mahmoodzadeh et al. [52], or a (commercially available) cooled sensor. Both solutions would increase drone payload and therefore reduce battery life. A software-based method detecting the sensor drift over multiple images would be less hardware-relevant, but its accuracy is still to be investigated: We found that the correction values are potentially comparatively large, which points to the risk of a large uncertainty contribution of these values. If the issues of automatic co-referencing of images and building models can be solved and a sufficiently accurate model of environmental conditions (in particular air temperature, surrounding radiation temperature, and wind) is created, the dynamic model calibration approach would allow for large-scale building envelope evaluations.

In the long term, referencing thermography and acoustic signals as image textures to the same building model could allow for large-scale multi-sensor analysis of thermal transmittance and airtightness as well as localization of heat bridges and air leakages.

## 4. Summary and conclusion

Our study contributes to the understanding of thermal losses in existing buildings by investigating two primary mechanisms: air exchange and heat conduction. To achieve an assessment of these losses across entire building envelopes, we focus on the potential of contact-less technologies that enable spatially resolved insights. Automated evaluation of the results is a key factor in ensuring the scalability and practical applicability of these methods.

Building up on previous research on the applicability of multiple contact-less measurement technologies for building energy assessments, we applied two innovative methods to an exemplary building complex: acoustic air leakage detection and drone-based quantitative infrared thermography. The chosen structure, characterized by different construction periods and heterogeneous insulation performance, provided an ideal test case for validating these novel measurement approaches.

The acoustic assessment of the airtightness, conducted using a sound source inside the building and an acoustic camera on the outside, demonstrated the feasibility of large-scale air leakage detection. To the best of our knowledge, this is the most comprehensive field study conducted so far. The method successfully identifies and visualizes potential leaks across large façade areas, with many detections confirmed through visual inspection. These results reinforce the method's applicability for assessing airtightness in large buildings and highlight its potential for further refinement and automation.

The drone-based thermography approach aimed to capture spatially distributed surface temperature data multiple times throughout a single night. While the method holds promise for large-scale thermal assessments, its practical application remains constrained by significant challenges, including image positioning accuracy, environmental influences, and calibration limitations. Future improvements in image processing, automated integration with building models, and enhanced thermal calibration protocols are essential to increase the reliability of this approach.

Despite the promising results and that both methods have shown to be applicable from a theoretical point of view, further research and development are necessary to transition these methods from experimental applications to practical tools for the building industry, not only regarding software and hardware interfaces between imaging sensors, building models, and boundary condition monitoring. Key areas for improvement in **airtightness assessment** include:

- Enhancing automation for leak detection, potentially using machine learning techniques.
- Developing quantitative evaluation metrics to complement qualitative assessments.
- Integrating results into building information models (BIM) for improved geometry analysis and visualization.

Regarding **drone-based quantitative thermography**, the main challenges to address are:

- Ensuring precise alignment of thermal images with building geometry.
- Improving calibration procedures for thermal images acquired in flight.
- Refining the connection between measured envelope temperatures and to dynamic thermal simulations, particularly in relation to wind effects on convective heat transfer.

If these challenges are successfully addressed, these methods could evolve from qualitative diagnostic tools to quantitative assessment techniques capable of feeding high-precision data into building performance simulations. This advancement would significantly enhance decision-making in energy retrofits as well as post-retrofit quality control. Ongoing research work focuses on refining these methods in controlled environments, such as laboratory-based airtightness measurement for the quantification of leaks and ground-based thermal imaging using vehicle-mounted sensors.

## Glossary

*Symbols*

| Symbol | Description | Unit |
|---|---|---|
| $h$ | Surface coefficient of heat transfer | $\mathrm{W\,m^{-2}\,K^{-1}}$ |
| $L$ | Radiance | $\mathrm{W\,sr^{-1}\,m^{-2}}$ |
| $T$ | Temperature (thermodynamic scale) | K |
| $U$ | U-value (thermal transmittance) | $\mathrm{W\,m^{-2}\,K^{-1}}$ |
| $\varepsilon$ | Emissivity | – |
| $\vartheta$ | Nadir angle | ° *or* rad |
| $\tau$ | Transmittance | – |
| $\varphi$ | Azimuth angle | ° *or* rad |

*Abbreviations and subscripts*

| Symbol | Description |
|---|---|
| ASS | Acoustic Assessment Score |
| atm | Atmosphere |
| bb | Black body |
| BIM | Building information model(ling) |
| cam | Camera |
| comb | Combined |
| IFC | Industry Foundation Classes (BIM standard) |
| IR | Infrared |
| IRT | Infrared thermography |
| MFAS | Multi-frequency Assessment Score |
| NTC | Negative temperature coefficient (device for temperature measurement) |
| o | Outgoing direction |
| QIRT | Quantitative infrared thermography |
| r | Reflected |
| RC | Resistance-capacitance |
| RTK-GPS | Real-time kinematic GPS |
| s | Surface |
| UAV | Unmanned aerial vehicle (“drone”) |

## CRediT authorship contribution statement

**Philip Groesdonk:** Writing – original draft, Project administration, Methodology, Investigation, Conceptualization. **Benedikt Kölsch:** Writing – original draft, Project administration, Methodology, Investigation, Conceptualization. **Björn Schiricke:** Writing – original draft, Methodology, Formal analysis. **Markus Diel:** Writing – review & editing, Formal analysis. **Nirav Patel:** Writing – original draft, Methodology, Investigation, Formal analysis. **Bernhard Hoffschmidt:** Writing – review & editing, Funding acquisition, Conceptualization.

## Funding

This work was conducted in the research project "Pilotanwendung von Gebäudetomograph-Messmethoden an einem Institut der Innovationsallianz Baden-Württemberg (Gtom-innBW)" which was funded by the Ministry of Economic Affairs, Labour and Tourism Baden-Württemberg, Germany under the grant number: WM3-4332-157/64.

## Declaration of competing interest

The authors declare the following financial interests/personal relationships which may be considered as potential competing interests: Bernhard Hoffschmidt reports financial support was provided by State Ministry of Baden-Wuerttemberg for Economic Affairs, Labour and Tourism. Benedikt Koelsch has patent #DE 10 2023 100 701 pending to Deutsches Zentrum für Luft- und Raumfahrt e.V. Benedikt Kölsch (as part-time employee) and Bernhard Hoffschmidt (as co-founder and board member) are involved with Lumoview Building Analystics GmbH, the company responsible for the production of the IFC model mentioned in the paper. Lumoview had no role in the design of the study, in the writing of the manuscript, or in the decision to publish the results. The other authors declare that they have no known competing financial interests or personal relationships that could have appeared to influence the work reported in this paper.

## Acknowledgments

The authors thank the "Hahn-Schickard-Gesellschaft für angewandte Forschung e.V". in Villingen-Schwenningen for providing their office buildings as test cases.

## Data availability

The authors do not have permission to share data.

## References

[1] European Commission, 'Fit for 55': Delivering the EU's 2030 Climate Target on the Way to Climate Neutrality, Brussels, 2021.
[2] European Commission, Comprehensive Study of Building Energy Renovation Activities and the Uptake of Nearly Zero-Energy Buildings in the EU – Final Report, Brussels, 2019.
[3] European Commission, EU Reference Scenario 2020 – Energy, Transport and GHG Emissions – Trends to 2050, Brussels, 2021.
[4] T. Konstantinou, B. Dimitrijević, Sustainable refurbishment for an adaptable built environment, in: S. Kosanović, T. Klein, T. Konstantinou, A. Radivojević, L. Hildebrand (Eds.), Sustainable and Resilient Building Design, in: Reviews of Sustainability and Resilience of the Built Environment for Education, Research and Design, TU Delft Open, Delft, 2018, pp. 207–227.
[5] P. van den Brom, A. Meijer, H. Visscher, Performance gaps in energy consumption: Household groups and building characteristics, Build. Res. Inf. 46 (1) (2018) 54–70, http://dx.doi.org/10.1080/09613218.2017.1312897.
[6] C. van Dronkelaar, M. Dowson, E. Burman, C. Spataru, D. Mumovic, A review of the energy performance gap and its underlying causes in non-domestic buildings, Front. Mech. Eng. 1 (2016) http://dx.doi.org/10.3389/fmech.2015.00017.
[7] Y. Bai, C. Yu, W. Pan, Systematic examination of energy performance gap in low-energy buildings, Renew. Sustain. Energy Rev. 202 (2024) 114701, http://dx.doi.org/10.1016/j.rser.2024.114701.
[8] P.X. Zou, X. Xu, J. Sanjayan, J. Wang, Review of 10 years research on building energy performance gap: Life-cycle and stakeholder perspectives, Energy Build. 178 (2018) 165–181, http://dx.doi.org/10.1016/j.enbuild.2018.08.040.
[9] T. Kalamees, Air tightness and air leakages of new lightweight single-family detached houses in Estonia, Build. Environ. 42 (6) (2007) 2369–2377, http://dx.doi.org/10.1016/j.buildenv.2006.06.001.
[10] J. Jokisalo, J. Kurnitski, M. Korpi, T. Kalamees, J. Vinha, Building leakage, infiltration, and energy performance analyses for Finnish detached houses, Build. Environ. 44 (2) (2009) 377–387, http://dx.doi.org/10.1016/j.buildenv.2008.03.014.
[11] J.M. Logue, M.H. Sherman, I.S. Walker, B.C. Singer, Energy impacts of envelope tightening and mechanical ventilation for the U.S. residential sector, Energy Build. 65 (2013) 281–291, http://dx.doi.org/10.1016/j.enbuild.2013.06.008.
[12] B. Jones, P. Das, Z. Chalabi, M. Davies, I. Hamilton, R. Lowe, A. Mavrogianni, D. Robinson, J. Taylor, Assessing uncertainty in housing stock infiltration rates and associated heat loss: English and UK case studies, Build. Environ. 92 (2015) 644–656, http://dx.doi.org/10.1016/j.buildenv.2015.05.033.
[13] W. Bracke, N. Van Den Bossche, A. Janssens, Airtightness of building penetrations: air sealing solutions, durability effects and measurement uncertainty, in: Proceedings of the 35th AIVC Conference, 2014.
[14] V. Leprince, A. Bailly, R. Carrié, M. Olivier, State of the art of non-residential buildings air-tightness and impact on the energy consumption, in: Proceedings of the 32nd AIVC Conference, 2011.
[15] E. Rodrigues, M.S. Fernandes, N. Soares, Á. Gomes, A.R. Gaspar, J.J. Costa, The potential impact of low thermal transmittance construction on the European design guidelines of residential buildings, Energy Build. 178 (2018) 379–390, http://dx.doi.org/10.1016/j.enbuild.2018.08.009.

[16] N. Abreu, A. Pinto, A. Matos, M. Pires, Procedural point cloud modelling in scan-to-BIM and scan-vs-BIM applications: A review, ISPRS Int. J. Geo-Inf. 12 (7) (2023) 260, http://dx.doi.org/10.3390/ijgi12070260.
[17] O. Spielhaupter, A. Mahdavi, Aspects of BIM-to-BEM information transfer: A tale of two workflows, in: R.J. Scherer, S.F. Sujan, E. Hjelseth (Eds.), ECPPM 2022 - EWork and EBusiness in Architecture, Engineering and Construction 2022, CRC Press, London, 2023, pp. 303–310, http://dx.doi.org/10.1201/9781003354222-39.
[18] ISO 9972, Thermal Performance of Buildings: Determination of Air Permeability of Buildings: Fan Pressurization Method, Technical standard, 2015.
[19] B. Kölsch, A. Mélois, V. Leprince, Improvement of the ISO 9972: Proposal for a more reliable standard to measure air leakage rate using the fan pressurisation method, in: Proceedings of the 13th International BuildAir-Symposium, Hannover, Germany, 2023.
[20] A. Mélois, F.R. Carrié, M. El Mankibi, B. Moujalled, Uncertainty in building fan pressurization tests: Review and gaps in research, J. Build. Eng. 52 (2022) 104455, http://dx.doi.org/10.1016/j.jobe.2022.104455.
[21] C. Ghazi, J. Marshall, A CO2 tracer-gas method for local air leakage detection and characterization, Flow Meas. Instrum. 38 (2014) 72–81, http://dx.doi.org/10.1016/j.flowmeasinst.2014.05.015.
[22] B. Kölsch, J. Pernpeintner, B. Schiricke, E. Lüpfert, Air leakage detection in building façades by combining lock-in thermography with blower excitation, Int. J. Vent. 22 (4) (2023) 357–365, http://dx.doi.org/10.1080/14733315.2023.2198791.
[23] ASTM E1186-17, Air Leakage Site Detection in Building Envelopes and Air Barrier Systems, Technical standard, 2017.
[24] D.N. Keast, H.-S. Pei, The use of sound to locate infiltration openings in buildings, in: Proceedings of the ASHRAE-DOE Conference on the Thermal Performance of the Exterior Envelope of Buildings, Orlando, FL, 1979.
[25] T. Sonoda, F. Peterson, A sonic method for building air-leakage measurements, Appl. Energy 22 (3) (1986) 205–224, http://dx.doi.org/10.1016/0306-2619(86)90003-6.
[26] M. Ringger, P. Hartmann, Evaluation of an acoustical method for detecting air leaks, Air Infiltration Rev. 11 (1) (1989) 6–9.
[27] O.A. Hassan, An alternative method for evaluating the air tightness of building components, Build. Environ. 67 (2013) 82–86, http://dx.doi.org/10.1016/j.buildenv.2013.05.007.
[28] A. Elsaei, M. Machimbarrena, A. Meiss, I. Poza-Casado, M. Padilla-Marcos, A multi-stage analysis of air leakage and acoustic performance on a full-scale test chamber, J. Build. Eng. 114 (2025) 114301, http://dx.doi.org/10.1016/j.jobe.2025.114301.
[29] V. Iordache, T. Catalina, Acoustic approach for building air permeability estimation, Build. Environ. 57 (2012) 18–27, http://dx.doi.org/10.1016/j.buildenv.2012.04.008.
[30] K. Varshney, J.E. Rosa, I. Shapiro, D. Scott, Air-infiltration measurements in buildings using sound transmission loss through small apertures, Int. J. Green Energy 10 (5) (2013) 482–493, http://dx.doi.org/10.1080/15435075.2012.675603.
[31] R.W. Graham, Infrasonic Impedance Measurements of Buildings for Air Leakage Determination (Master's thesis), Syracuse University, Syracuse, NY, 1977.
[32] N. Bader, P. Holstein, K. Eckert, H.-J. Münch, L. Holtkamp, T.d. van Eschut, Akustisches verfahren zur dichtheitsprüfung, in: B. Weller, S. Horn (Eds.), Denkmal Und Energie 2018, Springer Fachmedien Wiesbaden, Wiesbaden, 2017, pp. 285–295, http://dx.doi.org/10.1007/978-3-658-19672-1_22.
[33] P. Holstein, N. Bader, S. Moeck, H.-J. Münch, D. Döbler, A. Jahnke, Akustische verfahren zur ermittlung der luftdichtheit von bestandsgebäuden, in: B. Weller, L. Scheuring (Eds.), Denkmal Und Energie 2020, Springer Fachmedien Wiesbaden, Wiesbaden, 2020, pp. 111–123, http://dx.doi.org/10.1007/978-3-658-28753-5_8.
[34] B. Kölsch, B. Schiricke, E. Lüpfert, B. Hoffschmidt, Detection of air leakage in building envelopes using microphone arrays, in: Proceedings of the 41st AIVC - ASHRAE IAQ Joint Conference, 2022.
[35] B. Kölsch, B. Schiricke, J. Estevam Schmiedt, B. Hoffschmidt, Estimation of air leakage sizes in building envelope using high-frequency acoustic impulse response technique, in: Proceedings of the 40th AIVC Conference, 2019, pp. 80–89.
[36] B. Kölsch, I.S. Walker, B. Schiricke, W.W. Delp, B. Hoffschmidt, Quantification of air leakage paths: A comparison of airflow and acoustic measurements, Int. J. Vent. 22 (2) (2021) 101–121, http://dx.doi.org/10.1080/14733315.2021.1966576.
[37] G. Raman, M. Prakash, R.C. Ramachandran, H. Patel, K. Chelliah, Remote detection of building air infiltration using a compact microphone array and advanced beamforming methods, in: Proceedings of the BeBeC, 5th Berlin Beamforming Conference, Gesellschaft zur Förderung Angewandter Informatik, Berlin, 2014.
[38] K. Chelliah, G. Raman, R.T. Muehleisen, Enhanced nearfield acoustic holography for larger distances of reconstructions using fixed parameter tikhonov regularization, J. Acoust. Soc. Am. 140 (2016) 114–120, http://dx.doi.org/10.1121/1.4954757.
[39] K. Chelliah, G. Raman, R.T. Muehleisen, An experimental comparison of various methods of nearfield acoustic holography, J. Sound Vib. 403 (2017) 21–37, http://dx.doi.org/10.1016/j.jsv.2017.05.015.
[40] N. Janotte, B. Kölsch, E. Lüpfert, J. Pernpeintner, B. Schiricke, J. Estevam Schmiedt, D. Baumbach, A. Choinowski, D. Dahlke, I. Ernst, M. Linkiewicz, A. Schischmanow, S. Dill, T. Karrer, M. Peichl, D. Heuskin, Application of a combination of innovative non-destructive measurement techniques for structural, energetic and safety analysis of buildings, J. Build. Eng. 95 (2024) 109937, http://dx.doi.org/10.1016/j.jobe.2024.109937.
[41] P. Groesdonk, Interpretation of Remote Sensing Data for Energy Performance Assessments of Existing Buildings (Dissertation), RWTH Aachen, Aachen, 2024, http://dx.doi.org/10.18154/RWTH-2024-11518.
[42] D. Bienvenido-Huertas, J. Moyano, D. Marín, R. Fresco-Contreras, Review of in situ methods for assessing the thermal transmittance of walls, Renew. Sustain. Energy Rev. 102 (2019) 356–371, http://dx.doi.org/10.1016/j.rser.2018.12.016.
[43] ISO 6946, Building Components and Building Elements: Thermal Resistance and Thermal Transmittance: Calculation Methods, Technical standard, 2017.
[44] ISO 9869-1, Thermal Insulation: building Elements: In-Situ Measurement of Thermal Resistance and Thermal Capacitance: Heat Flow Meter Method, Technical standard, 2014.
[45] D. Patel, J. Estevam Schmiedt, M. Röger, B. Hoffschmidt, Approach for external measurements of the heat transfer coefficient (U-value) of building envelope components using UAV based infrared thermography, in: 14th Quantitative InfraRed Thermography Conference, QIRT, QIRT Council, Berlin, 2018, pp. 379–386, http://dx.doi.org/10.21611/qirt.2018.026.
[46] G. Dall'O', L. Sarto, A. Panza, Infrared screening of residential buildings for energy audit purposes: Results of a field test, Energies 6 (8) (2013) 3859–3878, http://dx.doi.org/10.3390/en6083859.
[47] R. Madding, Finding R-values of stud frame constructed houses with IR thermography, in: InfraMation 2008 Proceedings, 2008, pp. 261–277.
[48] N. Bayomi, S. Nagpal, T. Rakha, J.E. Fernandez, Building envelope modeling calibration using aerial thermography, Energy Build. 233 (2021) 110648, http://dx.doi.org/10.1016/j.enbuild.2020.110648.
[49] M. Videras Rodríguez, S. Gómez Melgar, J.M. Andújar Márquez, Evaluation of aerial thermography for measuring the thermal transmittance (U-value) of a building façade, Energy Build. 324 (2024) 114874, http://dx.doi.org/10.1016/j.enbuild.2024.114874.
[50] D. Patel, J. Estevam Schmiedt, M. Röger, B. Hoffschmidt, A model calibration approach to U-value measurements with thermography, Buildings 13 (9) (2023) 2253, http://dx.doi.org/10.3390/buildings13092253.
[51] M. Mahmoodzadeh, V. Gretka, I. Lee, P. Mukhopadhyaya, Infrared thermography for quantitative thermal performance assessment of wood-framed building envelopes in Canada, Energy Build. 258 (2022) 111807, http://dx.doi.org/10.1016/j.enbuild.2021.111807.
[52] M. Mahmoodzadeh, V. Gretka, P. Mukhopadhyaya, Challenges and opportunities in quantitative aerial thermography of building envelopes, J. Build. Eng. 69 (2023) 106214, http://dx.doi.org/10.1016/j.jobe.2023.106214.

[53] J.R. Schott, J.D. Biegel, E.P. Wilkinson, Quantitative aerial survey of building heat loss, in: G.E. Courville (Ed.), Thermosense V, in: SPIE Proceedings, SPIE, 1983, pp. 187–195, http://dx.doi.org/10.1117/12.934479.
[54] J.R. Schott, Methods for estimation of and correction for atmospheric effects on remotely sensed data, in: A. Kohnle, W.B. Miller (Eds.), Atmospheric Propagation and Remote Sensing II, in: SPIE Proceedings, SPIE, 1993, pp. 448–482, http://dx.doi.org/10.1117/12.154850.
[55] FLIR, The ultimate infrared handbook for R&D professionals: A resource guide for using infrared in the research and development industry, 2023, URL: https://www.flirmedia.com/MMC/THG/Brochures/T559243/T559243_EN.pdf.
[56] T. Rakha, Y. El Masri, K. Chen, E. Panagoulia, P. de Wilde, Building envelope anomaly characterization and simulation using drone time-lapse thermography, Energy Build. 259 (2022) 111754, http://dx.doi.org/10.1016/j.enbuild.2021.111754.
[57] B. Schiricke, M. Diel, B. Kölsch, Field testing of an acoustic method for locating air leakages in building envelopes, Buildings 14 (4) (2024) http://dx.doi.org/10.3390/buildings14041159.
[58] Lumoview Building Analytics GmbH, Digitization of buildings in 2 seconds: Lumoview Building Analytics GmbH, 2024, URL: https://www.lumoview.com.
[59] E. Fichter, Automatisierte Erzeugung geometrischer Modelle für die BIM-basierte Gebäudesimulation (Dissertation), RWTH Aachen, Aachen, 2022, http://dx.doi.org/10.18154/RWTH-2022-11049.
[60] D. Ekaso, F. Nex, N. Kerle, Accuracy assessment of real-time kinematics (RTK) measurements on unmanned aerial vehicles (UAV) for direct geo-referencing, Geo-Spatial Inf. Sci. 23 (2) (2020) 165–181, http://dx.doi.org/10.1080/10095020.2019.1710437.
[61] Agisoft, Thermal imagery processing, 2023, URL: https://agisoft.freshdesk.com/support/solutions/articles/31000158942-thermal-imagery-processing.
[62] P. Gorzalka, J. Estevam Schmiedt, J. Göttsche, B. Hoffschmidt, M. Linkiewicz, D. Patel, S. Plattner, C. Schorn, D. Frommholz, Remote sensing for building energy simulation input – A field trial, in: V. Corrado, E. Fabrizio, A. Gasparella, F. Patuzzi (Eds.), Proceedings of Building Simulation 2019: 16th Conference of IBPSA, in: Building Simulation Conference proceedings, IBPSA, 2020, pp. 4094–4101, http://dx.doi.org/10.26868/25222708.2019.210186.
[63] M. Vollmer, K.-P. Möllmann, Infrared Thermal Imaging: Fundamentals, Research and Applications, second ed., Wiley-VCH, Weinheim, 2018, http://dx.doi.org/10.1002/9783527693306.
[64] P.A. Fokaides, S.A. Kalogirou, Application of infrared thermography for the determination of the overall heat transfer coefficient (U-value) in building envelopes, Appl. Energy 88 (12) (2011) 4358–4365, http://dx.doi.org/10.1016/j.apenergy.2011.05.014.
[65] G. Gaussorgues, Infrared Thermography, Microwave technology series, vol. 5, Chapman & Hall, London, 1994.
[66] M. Diel, B. Schiricke, J. Pernpeintner, Test facility for building envelope leakage type analysis and improvement of acoustic and thermographic airtightness measurement methods, in: Proceedings of the 44th AIVC -12th TightVent & 10th Venticool Conference, 2024.